Journal of Power Sources 234 (2013) 244–251

Contents lists available at SciVerse ScienceDirect

Journal of Power Sources

journal homepage: www.elsevier.com/locate/jpowsour

Double-perovskite $PrBaCo_{2/3}Fe_{2/3}Cu_{2/3}O_{5+\delta}$ as cathode material for intermediate-temperature solid-oxide fuel cells

Fangjun Jin [a], Yu Shen [a,b], Rui Wang [a], Tianmin He [a,*]

[a] Key Laboratory of Physics and Technology for Advanced Batteries, Ministry of Education, College of Physics, Jilin University, Changchun 130012, PR China
[b] School of Materials Science and Engineering, Changchun University of Science and Technology, Changchun 130022, PR China

HIGHLIGHTS

- A single-phase double-perovskite $PrBaCo_{2/3}Fe_{2/3}Cu_{2/3}O_{5+\delta}$ (PBCFC) is prepared by the EDTA–citrate complexing method.
- XPS analysis shows that the Pr^{3+}/Pr^{4+}, Co^{3+}/Co^{4+}, Fe^{3+}/Fe^{4+}, Cu^{+}/Cu^{2+} and Ba^{2+} species coexist in the PBCFC.
- PBCFC material has a good chemical compatibility with SDC and GDC electrolytes below 900 °C and 950 °C, respectively.
- Partial substitution of Fe and Cu for Co efficiently lowers the thermal expansion coefficient of the PBCFC.
- Low polarization resistance of 0.071 Ω cm^2 and high power density of 512 mW cm^{-2} at 750 °C are obtained on GDC electrolyte.

ARTICLE INFO

Article history:
Received 16 November 2012
Received in revised form
25 January 2013
Accepted 30 January 2013
Available online 6 February 2013

Keywords:
Solid-oxide fuel cell
Double-perovskite cathode
Chemical compatibility
Electrochemical performance
Thermal expansion
XPS

ABSTRACT

Double-perovskite $PrBaCo_{2/3}Fe_{2/3}Cu_{2/3}O_{5+\delta}$ (PBCFC) is synthesized by the EDTA–citrate complexing method, and investigated as a novel cathode material for CeO_2-based intermediate-temperature solid-oxide fuel cells (IT-SOFCs). The PBCFC material exhibits good chemical compatibility with $Ce_{0.8}Sm_{0.2}O_{1.9}$ (SDC) and $Ce_{0.9}Gd_{0.1}O_{1.95}$ (GDC) electrolytes at 900 and 950 °C for 10 h, respectively. XPS analysis shows that the rare-earth and transition-metal cations in the double-perovskite PBCFC exist in two different valence states, i.e., $[Pr^{3+}/Pr^{4+}][Ba^{2+}][Co^{3+}/Co^{4+}]_{2/3}[Fe^{3+}/Fe^{4+}]_{2/3}[Cu^{+}/Cu^{2+}]_{2/3}O_{5+\delta}$. The electrical conductivity of the PBCFC sample reaches a maximum of 144 S cm^{-1} at 600 °C in air. The thermal expansion coefficient (TEC) of the PBCFC sample is 16.6 × 10^{-6} K^{-1} between 30 and 850 °C in air. The polarization resistance of the PBCFC cathode on SDC and GDC electrolytes are 0.144 and 0.038 Ω cm^2 at 800 °C, respectively. The maximum power densities of a single cell with the PBCFC cathode on a 300 μm-thick GDC electrolyte are 659 and 512 mW cm^{-2} at 800 and 750 °C, respectively. Fe and Cu co-doped $PrBaCo_2O_{5+\delta}$ exhibits decreased TEC and improved electrochemical performance, making it a suitable cathode material for GDC electrolyte IT-SOFCs.

1. Introduction

A solid-oxide fuel cell (SOFC) is an electrochemical energy conversion device with low levels of pollutants and high energy conversion efficiency. SOFCs provide the most efficient means to convert the chemical energy stored in fuel directly into usable electrical energy [1]. Traditional SOFCs are operated at high temperatures up to approximately 1000 °C. Thus, reactions among materials and high temperature sealing occur, which lead to high costs of materials and SOFC fabrication. SOFCs with reduced operating temperatures from the traditional ~1000 °C to 600–800 °C, i.e., intermediate-temperature SOFCs (IT-SOFCs), can significantly decrease production cost and improve the long-term stability of SOFC systems. However, the electrocatalytic activity of traditional cathodes significantly decreases because of the reduced SOFC operating temperature [2]. As a result, the electrode polarization resistance increases and limits the current output of the whole cell, leading to a marked decrease in SOFC performance [3,4]. Therefore, appropriate cathode materials with acceptable electrochemical activity and power density within the intermediate-temperature range (600–800 °C) should be developed.

In SOFCs, one of the main requirements for the cathode is a high reaction rate for oxygen reduction. Over the last few years, the performance of IT-SOFC cathodes has been extensively studied. Ferrites, cobaltites, and ferrite–cobaltite perovskites are the most commonly used materials, including perovskite cathode materials

* Corresponding author. Tel.: +86 431 85166112; fax: +86 431 85167827.
E-mail addresses: hetm@jlu.edu.cn, hly@mail.jlu.edu.cn (T. He).

0378-7753/$ – see front matter © 2013 Elsevier B.V. All rights reserved.
http://dx.doi.org/10.1016/j.jpowsour.2013.01.172

$Ln(Ba,Sr)(Co,Fe)O_{3-\delta}$ (Ln = La, Pr, Nd, and Gd) [5–10] and double-perovskite cathode materials $LnBaCo_2O_{5+\delta}$ (Ln = La, Pr, Nd, Sm, Gd and Y) [11–15]. Most of them show high feasibility as cathodes for IT-SOFCs. Many cobalt-containing perovskite materials are generally mixed ionic–electronic conductors (MIECs), which can extend the electrochemical active area (i.e., increase the active three-phase boundary length). In particular, cobalt-based double-perovskite MIECs ($AA'Co_2O_{5+\delta}$) reportedly have good electrocatalytic activity as cathodes for IT-SOFCs because their alternating lanthanide and alkali-earth planes can reduce the oxygen bonding strength and increase the oxygen diffusivity [16]. This characteristic improves the electrochemical performance of the cathodes. Kim et al. [17] reported that $PrBaCo_2O_{5+\delta}$ (PBCO) exhibits high oxygen diffusion and surface-exchange kinetics, which are two to three orders of magnitude higher than those of $GdBaCo_2O_{5+\delta}$ (GBCO) under the same conditions. These findings indicate that PBCO has a higher cathode performance than GBCO. This deduction has been thoroughly verified experimentally by Zhang et al. [11], who found that PBCO exhibits the best cathode performance in $LnBaCo_2O_{5+\delta}$ (Ln = La, Pr, Nd, Sm, Gd, and Y) materials. The polarization resistance of this cathode on $Ce_{0.8}Sm_{0.2}O_{1.9}$ (SDC) electrolyte is 0.213 Ω cm^2 at 600 °C. In addition, cathode materials introducing Pr^{3+} reportedly have higher electrical conductivity and lower overpotential values because of the Pr^{3+}/Pr^{4+} valence change [18]. Recently, Chen et al. [15] reported a thin-film SDC electrolyte fuel cell with a PBCO cathode that exhibits low polarization resistance and high power density, i.e., 0.4 Ω cm^2 and 620 mW cm^{-2} at 600 °C, respectively. These values indicate that the PBCO material is a promising cathode for IT-SOFCs.

However, the widespread application of cobalt-based perovskite cathode materials is challenged by their high thermal expansion coefficient (TEC), high cobalt cost, and low long-term chemical stability. All these factors are related with the spin-state transition of octahedral-site Co^{3+} ions, the formation of oxygen vacancies, and the weak bonding energy of the Co–O bond [19,20]. For example, the TEC of PBCO cathode is 21.5 × 10^{-6} K^{-1} between 30 and 1000 °C [12], which is much higher than that of common electrolyte materials. From the perspective of thermal expansion compatibility, the TEC mismatch limits its application at high temperatures. Therefore, a better approach to overcoming the above problems may be the use of TEC cathode materials compatible with SOFC components. Previous studies have indicated that the replacement of one transition-metal ion by another significantly affects the thermal expansion and electrochemical performances of cathodes. For example, Qiu et al. [21] reported that the TEC of $Ln_{1-x}Sr_xCo_{1-y}Fe_yO_{3-\delta}$ cathodes decreases with increased Fe content. Zhao et al. [22] and Zhou et al. [23] reported that the substitution of Fe or Cu for Co sites in $LnBaCo_2O_{5+\delta}$ materials improves the cathode performance and decreases the TECs. Jo et al. [24] reported that Fe and Cu co-doped $GdBaCo_2O_{5+\delta}$ has a low TEC of 14.6 × 10^{-6} K^{-1} between 30 and 900 °C, and a low polarization resistance of 0.048 at 750 °C on a $Ce_{0.9}Gd_{0.1}O_{1.95}$ (GDC) electrolyte. Zhou et al. [25] have also shown that Fe and Cu co-doping for Co sites lowers the TEC of $GdBaCuCo_{0.5}Fe_{0.5}O_{5+\delta}$ (GBCCF) compared with GBCO cathode. The main reason is that partial substitution of Fe and Cu for Co sites can lower the cobalt contents and relative amount of the spin-state transition in Co^{3+} ions from low to high spin. In addition, the substitutions of transition-metal ions for Co in cobalt-based perovskite cathodes have also reduced the costs of SOFC application. Fe and Cu co-doped $LnBaCo_2O_{5+\delta}$ (Ln = Sm and Gd) double-perovskites have been investigated as potential cathode materials for IT-SOFCs. However, the effects of Fe and Cu co-doping on the structure and properties of the PBCO double-perovskite have not yet been reported.

In this work, a novel double-perovskite, $PrBaCo_{2/3}Fe_{2/3}Cu_{2/3}O_{5+\delta}$ (PBCFC), is synthesized by the EDTA–citrate complexing method. The chemical compatibility of PBCFC with SDC and GDC electrolytes at different temperatures is examined. The effects of Fe and Cu double-doping on the structure and properties of the PBCFC material are investigated. The electrochemical performances of the PBCFC cathode on CeO_2-based electrolytes were also tested.

2. Experimental

2.1. Material synthesis, cell fabrication, and tests

Double-perovskite PBCFC powders were prepared by the EDTA–citrate complexing method. A stoichiometric amount of Pr_6O_{11} was dissolved in nitric acid to form a nitrate. This nitrate was then mixed with the metal nitrates $Ba(NO_3)_2$, $Co(NO_3)_2 \cdot 6H_2O$, $Fe(NO_3)_3 \cdot 9H_2O$, and $Cu(NO_3)_2 \cdot 6H_2O$ in deionized water. The Pr_6O_{11} powders were preheated at 900 °C for 2 h prior to use. According to the cation stoichiometry of the precursor, the nitrates were mixed with citric acid and EDTA to form a metal complex through inorganic polymerization reactions. $NH_3 \cdot H_2O$ was added as an assistant reagent to adjust the pH. The mixed solution gradually became a homogeneous black viscous gel as water evaporated by heating and stirring. Dried powders were obtained by drying the samples at 180 °C for 4 h in an oven. Then, the resulting powders were heated at 600 and 900 °C for 4 and 10 h in air, respectively. The powders were pelletized and subsequently sintered at 950 °C for 10 h in air to obtain the final products in the desired PBCFC phase. SDC, GDC, and NiO powders were synthesized through the glycine-nitrate process. Dense SDC and GDC pellets approximately 13 mm in diameter were prepared by using uni-axial mold pressing powders at 220 MPa and by sintering at 1400 °C for 10 h in air.

The thickness of the sintered electrolyte pellets was controlled at 300 μm each by wet grinding with a waterproof abrasive paper. To prepare the symmetrical cell, the cathode slurry was applied on both sides of the electrolyte pellets using a screen-printing method. The symmetrical cells were then calcined at 900 or 950 °C for 4 h in air. Silver paste was painted on the electrodes as a current collector. The impedance spectra were tested from 600 °C to 800 °C using an electrochemical analyzer (CHI604D, Chenhua). NiO and GDC were mixed at a weight ratio of 65:35 as anode powders. The anode slurry was printed onto the GDC electrolyte and calcined at 1250 °C for 4 h. The cathode was printed onto the opposite side of GDC electrolyte and calcined at 950 °C for 4 h. The cell configuration was NiO–GDC/GDC/PBCFC, which was sealed onto one end of an alumina tube by silver paste. The cathode was exposed to ambient air, whereas dry hydrogen was fed to the anode chamber at a flow rate of 100 mL min^{-1}. The cell performance was tested from 600 °C to 800 °C with a four-electrode method using an electrochemical analyzer.

2.2. Material characterization

The crystalline structure and chemical compatibility of the PBCFC sample were examined using an X-ray diffractometer (Rigaku-D-Max γA; Cu Kα radiation, λ = 0.15418 nm) within an angular range of 20°–80° at 0.02° increments in 2θ at room temperature. The microstructure of the sintered sample was examined using a SEM system (JEOL JSM-6480LV). The chemical composition of the PBCFC sample was examined using an EDX system (EDAX CDU). XPS measurements were performed using a VG Scientific ESCALAB MK II X-ray photoelectron spectrometer and an Al Kα (1486.6 eV) radiation source. The base pressure of the sample chamber was 1.97 × 10^{-9} Torr. The binding energies were calibrated using the C 1s peak at 284.6 eV as a reference, and quoted with

a precision of ±0.2 eV. TEC measurement was performed using a dilatometer (Netzsch DIL 402C) from 30 °C to 850 °C with Al_2O_3 as a reference under an air-purge flow rate of 60 mL min^{-1} and heating rate of 5 °C min^{-1}. TGA was performed using a HENVEN HCT-3 instrument between 30 and 950 °C at a heating rate of 10 °C min^{-1} in air. Electrical conductivity was measured using the van der Pauw method from 300 °C to 850 °C in air.

3. Results and discussion

3.1. Crystal structure and chemical compatibility

Fig. 1(a) and (b) shows the XRD patterns of the PBCFC samples sintered at 900 and 950 °C for 10 h, respectively. For comparison, the XRD pattern of PBCO prepared by solid-state reaction is also shown in Fig. 1(c). PBCFC oxide has a single-phase double-perovskite structure without any attributable impurities, as shown in Fig. 1(a) and (b). The diffraction peaks are indexed within a tetragonal structure with the space group *P4/mmm* at room temperature. The effect of sintering temperatures on the degree of crystallinity of the PBCFC phase is also estimated. As shown in Fig. 1(a), the sample sintered at 900 °C for 10 h is indexed as a single-phase tetragonal structure. However, the XRD peak splits at (110), (102), (212), and (114) planes are not sharp as observed in Fig. 1(a). The degree of crystallinity of the PBCFC phase increases with increased temperature, as shown in Fig. 1(b), where clear peak splitting occurs at the (110), (102), (212), and (114) planes in the XRD pattern. These findings suggest that the sample sintered at 950 °C for 10 h has a high degree of crystallinity, exhibiting the typical tetragonal structure of a double-perovskite [26,27]. In view of the good degree of crystallinity, the properties of the samples sintered at 950 °C for 10 h are discussed in the following sections.

The microstructure and elemental composition of the PBCFC sample are characterized by SEM and EDX microanalysis. Fig. 2(a) and (b) shows the SEM and EDX of the PBCFC sample sintered at 950 °C for 10 h. Fig. 2(a) shows that the PBCFC sample is dense, implying that the sintering temperature established in this study is desirable. The size distribution of grains is homogeneous, and the average grain size is 1–3 μm. Fig. 2(b) indicates that only the Pr, Ba, Co, Cu, Fe, and O components are detected by EDX on the sample surface, and no impurities are observed. This finding well agrees with the XRD analysis result. The inset table in Fig. 2(b) shows the measured elemental composition of the sample surface. Obviously,

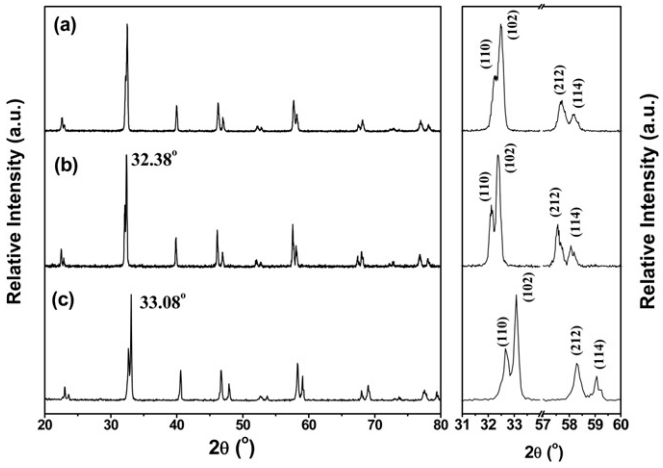

Fig. 1. XRD patterns of the PBCFC samples sintered at (a) 900 and (b) 950 °C for 10 h, respectively, and (c) XRD patterns of the PBCO sample prepared by a solid-state reaction.

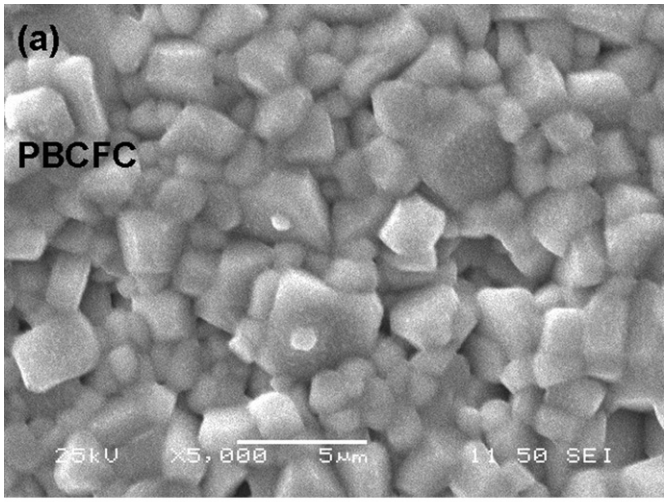

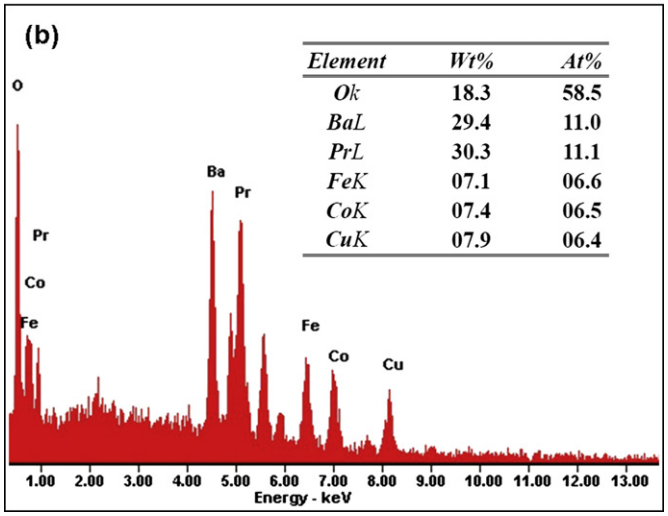

Element	Wt%	At%
Ok	18.3	58.5
BaL	29.4	11.0
PrL	30.3	11.1
FeK	07.1	06.6
CoK	07.4	06.5
CuK	07.9	06.4

Fig. 2. SEM image and EDX spectrum of the PBCFC sample sintered at 950 °C for 10 h.

the Pr:Ba and Co:Fe:Cu molar ratios are very close to the nominal stoichiometric compositions. The experimental results are in quantitative agreement with the nominal values. This result indicates that PBCFC oxide with a stoichiometric composition is obtained.

The unit-cell parameters are calculated from the XRD patterns in Fig. 1(b). For a tetragonal structure, the unit-cell parameters of PBCFC are as follows: $a = 0.39043$ nm, $c = 0.76507$ nm, and cell volume $V = 0.11663$ nm^3. The unit-cell volume of PBCFC is slightly larger than that of PBCO cathode [27]. Considering that the effective ionic radii of Fe and Cu are larger than those of Co [28], the substitution of Fe and Cu for Co sites induces lattice expansion, resulting in increased cell volume. In addition, a comparison of the XRD patterns in Fig. 1(b) and (c) shows that the diffraction peaks of PBCFC shift toward the slightly lower values of 2θ, suggesting that the cell volume indeed increases.

Fig. 3 shows the XRD patterns of the PBCFC–SDC and PBCFC–GDC mixtures (at 1:1 weight ratio) calcined at different temperatures. As shown in Fig. 3(a), several new diffraction peaks are observed in the XRD patterns of the PBCFC–SDC mixture after sintering at 950 °C for 10 h. They can be indexed as the new phases of Pr_2CuO_4 (JCPDS #79-0958) and $SmCu_2O_4$ (JCPDS #87-1744). This result shows that the PBCFC material is not compatible with SDC electrolyte above 950 °C. However, no obvious chemical reaction is observed between PBCFC and SDC, as shown Fig. 3(b). This finding

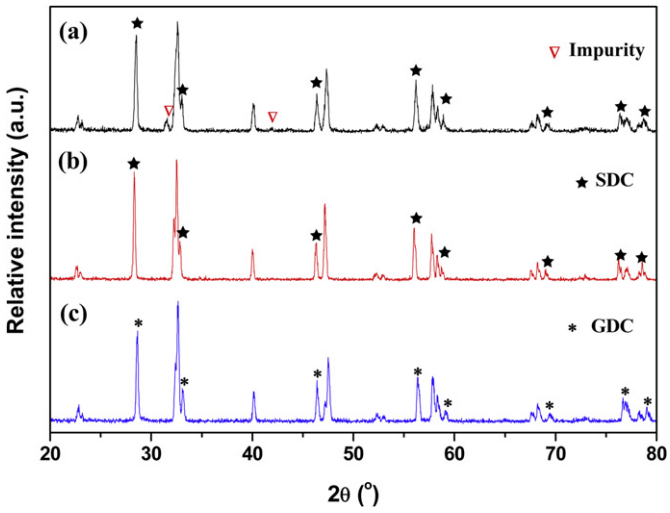

Fig. 3. XRD patterns of PBCFC–SDC(GDC) mixtures calcined at different temperatures: (a) PBCFC–SDC powders calcined at 950 °C for 10 h, (b) PBCFC–SDC powders calcined at 900 °C for 10 h, and (c) PBCFC–GDC powders calcined at 950 °C for 10 h.

indicates that PBCFC and SDC still maintain their respective structures in the PBCFC–SDC mixture after sintering at 900 °C for 10 h. This finding suggests that PBCFC is a chemically stable cathode material on SDC electrolyte below 900 °C. Fig. 3(c) shows that PBCFC and GDC coexist in their respective crystalline phases; no additional diffraction peaks and apparent peak shifts in the diffraction peaks are observed. This finding suggests that PBCFC oxide is chemically compatible with GDC electrolyte below 950 °C.

3.2. XPS analysis

XPS spectroscopy is an important technique widely used to study the chemical state and surface properties of materials. To describe the different spectral features of the PBCFC sample, the O 1s, Pr 3d, Fe 2p, Co 2p, Cu 2p, and Ba 3d core-level spectra are obtained, as shown in Figs. 4–6. All XPS spectra are fitted with a Shirley-type background subtraction method. The background-corrected XPS spectra are fitted by 80% Gaussian and 20% Lorentz functions for different chemical states of the elements. Fig. 4 shows that the O 1s core-level spectra show two peaks with binding

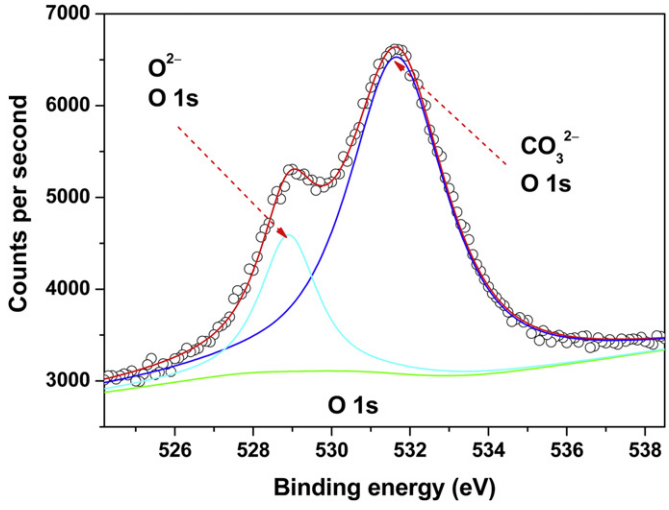

Fig. 4. XPS spectra (open circles) and fitted lines of O 1s in the PBCFC sample at room temperature.

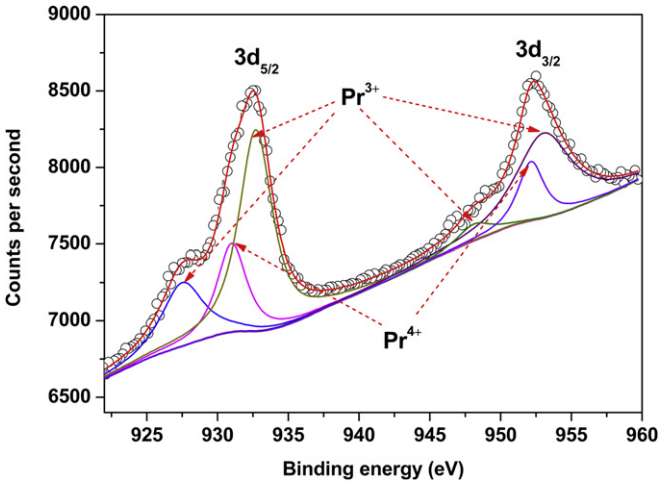

Fig. 5. XPS spectra (open circles) and fitted lines of Pr 3d in the PBCFC sample at room temperature.

energies of 531.6 and 528.9 eV, respectively. The peak at 531.6 eV is probably due to hydroxyl groups and carbonate compounds (O_H), whereas the other peak at 528.9 eV corresponds to the oxygen lattice (O_L) [29]. The O_L/O_H atomic ratio is 0.25. This observation can be attributed to the low valence states of transition-metal and alkaline-earth-metal elements in PBCFC and to the formation of oxygen vacancy that leads to a reduction in the amount of lattice oxygen. However, CO_2, hydroxide, and chemical absorption on the sample surface leads to the formation of the hydroxyl groups and carbonate film on the surface. Notably, the effect caused by the hydroxyl groups and carbonate compounds is negligible, as demonstrated by the XRD results.

Fig. 5 shows the Pr 3d core-level XPS spectra of the PBCFC sample. The Pr 3d peaks that envelope the Pr^{3+} and Pr^{4+} oxidation states are fitted in Fig. 5. The two characteristic peaks of Pr^{4+} $3d_{5/2}$ and $3d_{3/2}$ are observed at 931.0 and 952.1 eV, respectively. The peak pairs of 927.5/932.7 eV at $3d_{5/2}$ and 948.1/953.0 eV at $3d_{3/2}$ can be assigned to Pr^{3+}. Similar results have been previously observed [30,31], indicating that the oxidation states of Pr in the compound are 3+ and 4+.

Fig. 6(a) shows the fitted core-level spectrum results of Fe 2p for the PBCFC sample. The spin-orbit splitting in the Fe 2p XPS spectra shows a doublet of $2p_{3/2}$ and $2p_{1/2}$ excitation. The main peaks at 710.2 and 712.8 eV are representative of Fe^{3+} ($2p_{3/2}$) and Fe^{4+} ($2p_{3/2}$), whereas the peaks at 723.3 and 725.6 eV are representative of Fe^{3+} ($2p_{1/2}$) and Fe^{4+} ($2p_{1/2}$), respectively. The satellite peak around 719.4 eV can be assigned to the Fe^{3+} species. This finding agrees with that of Ghaffari et al. [32]. The estimated Fe^{4+}/Fe^{3+} atomic ratio is 35:65, as shown in Table 1.

Fig. 6(b) shows the Co 2p core-level XPS spectra of the PBCFC sample. The Co 2p core-level spectra of PBCFC show four peaks at $2p_{3/2}$ and $2p_{1/2}$ excitations. The corresponding binding energies are 778.8 and 780.5 eV at $2p_{3/2}$ and 794.1 and 796.0 eV at $2p_{1/2}$. These results indicate the existence of different valence states of cobalt ions on the PBCFC sample surface, which can be designated as the valence states of Co^{3+} and Co^{4+}. The most intense doublet at 778.8 and 794.1 eV can be assigned to Co^{3+} species, whereas the binding energies at 780.5 and 796.0 eV are considered as features of Co^{4+} species [33–35]. No high binding energy satellites at 785.0–788.0 eV are observed in the Co 2p core-level XPS spectra, indicating the absence of Co^{2+} species [36]. The binding energies of Co $2p_{3/2}$ and Co $2p_{1/2}$ are listed in Table 1. The atomic ratio of Co^{4+}/Co^{3+} is 45:55.

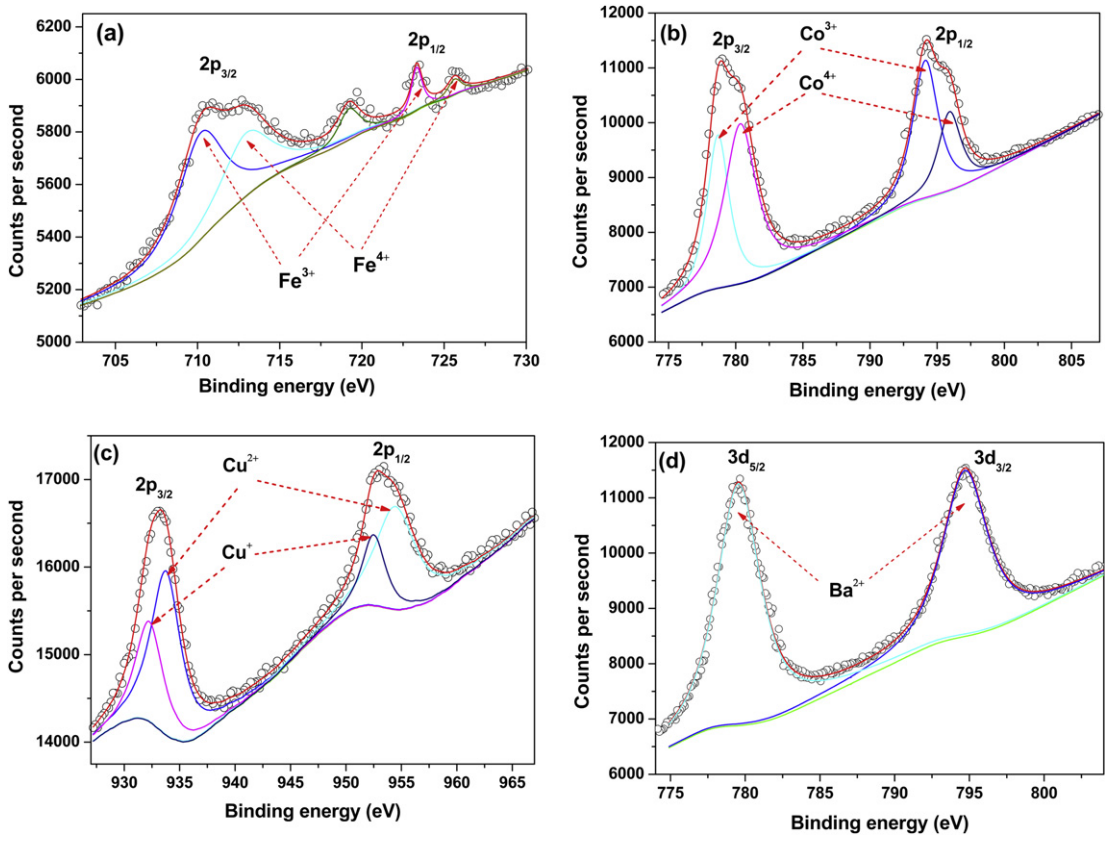

Fig. 6. XPS spectra (open circles) and fitted lines of (a) Fe 2p, (b) Co 2p, (c) Cu 2p, and (d) Ba 3d in the PBCFC sample at room temperature.

Fig. 6(c) and Table 1 show the XPS results of the Cu 2p core-level spectra at $2p_{3/2}$ and $2p_{1/2}$ of the PBCFC sample. The characteristic peaks of Cu^{+} and Cu^{2+} are 932.3 and 933.8 eV at $2p_{3/2}$ and 952.5 and 954.4 eV at $2p_{1/2}$ [37,38]. The Cu^{+}/Cu^{2+} atomic ratio is 31:69. The Ba 3d core-level XPS spectrum of the PBCFC sample is shown in Fig. 6(d). Only one chemical state of barium is found in the sample, indicating that the contribution to the spectra of pure Ba–O structure originates from double-perovskite PBCFC as well as minor barium carbonate and hydroxyl groups.

The XPS results clearly indicate the existence of Pr^{3+}/Pr^{4+}, Fe^{3+}/Fe^{4+}, Co^{3+}/Co^{4+}, Cu^{+}/Cu^{2+}, and Ba^{2+} species in the PBCFC sample. As described above, the average valences of transition-metal cations in double-perovskite PBCFC are lower than 3+. To maintain the electrical neutrality of PBCFC, the reduction in positive charge can be balanced by the formation of oxygen vacancies in oxygen lattices. Hence, the presence of a mixed valence of Pr, Fe, Co, and Cu in the pervoskite lattice may enhance the electronic conductivity and oxidation–reduction reaction rate in the cathodic atmospheres of an SOFC.

Table 1
Binding energies and percentage contributions of the core electrons for Fe, Co, and Cu from XPS.

Element		Binding energy (eV)		A^x/A_{all} (%)
		$2p_{3/2}$	$2p_{1/2}$	
Fe	Fe^{3+}	710.2	723.3	65
	Fe^{4+}	712.8	725.6	35
Co	Co^{3+}	778.8	794.1	55
	Co^{4+}	780.5	796.0	45
Cu	Cu^{2+}	933.8	954.4	69
	Cu^{+}	932.3	952.5	31

Note: A_{all}, all total A (Fe, Co, or Cu) atoms on the surface.

3.3. Thermal expansion behavior and TGA

Fig. 7 shows the thermal expansion curve and its differential curve for the PBCFC material. For comparison, the thermal expansion curves of PBCO [12] and $PrBaCoFeO_{5+\delta}$ (PBCF) cathodes are also shown. The thermal expansion curve of the PBCFC sample shows a linear dependence on temperature within the studied temperature range. The differential curve of $\Delta L/L_o$ vs. temperature for PBCFC demonstrates no abrupt change within this temperature range. The

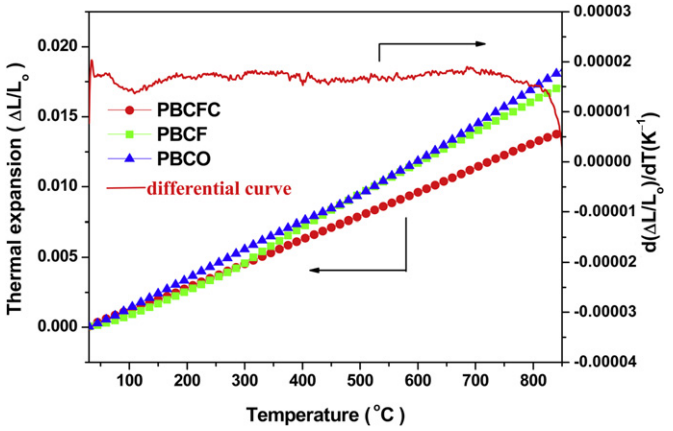

Fig. 7. Thermal expansion curves of the PBCFC, PBCF, and PBCO [12] samples between 30 and 850 °C in air, and the differential curves of the PBCFC sample.

average TEC of the PBCFC sample is 16.6×10^{-6} K^{-1} between 30 and 850 °C, whereas the average TECs of the PBCO and PBCF samples are 21.5×10^{-6} [12] and 21.0×10^{-6} K^{-1} between 30 and 1000 °C. Clearly, the average TEC of the PBCFC sample is lower than those of the PBCO and PBCF samples.

As mentioned in Section 1 (Introduction), the TEC of the cobalt-based perovskite cathodes is closely related to the Co content, metallic cation radii, and formation of oxygen vacancies [19,20]. The high TECs of cobalt-based perovskite cathodes are attributable to the spin-state transition of Co^{3+} ions with increased temperature. Fig. 7 shows that the Co content significantly affects the TECs of the cathodes. The TECs gradually decrease with decreased Co content. The reduced TECs for PBCFC cathode are due to the substitution of Fe and Cu for the Co sites in PBCO, resulting in decreased Co content and spin-state transition of Co^{3+} ions. Furthermore, the Fe–O bond is stronger than the Co–O bond, which leads to increased bonding energy with decreased Co content such that TEC decreases [39]. Similar studies have shown that Fe and Cu co-doping for Co sites reduce the TECs of $LnBaCo_{2/3}Fe_{2/3}Cu_{2/3}O_{5+\delta}$ cathodes (Ln = Sm and Gd) [24,40]. For example, the TEC values are 16.6×10^{-6} for $SmBaCo_{2/3}Fe_{2/3}Cu_{2/3}O_{5+\delta}$ [40] and $14.6 \times 10^{-}$ K^{-1} for $GdBaCo_{2/3}Fe_{2/3}Cu_{2/3}O_{5+\delta}$ [24], which are significantly lower than those of SBCO (19.1×10^{-6} K^{-1}) and GBCO (16.7×10^{-6} K^{-1}) cathodes [12].

Fig. 8 presents the TGA curve for the PBCFC sample upon heating in air. A small mass loss is observed in the curve at 30–340 °C, which may be associated with the desorption of moisture, carbon dioxide, and oxygen. Above 340 °C, the TGA curve shows an abrupt mass loss, which is due to the loss of lattice oxygen in the PBCFC sample. Meanwhile, the formation of oxygen vacancies is accompanied by a reduction of Fe^{4+}/Co^{4+} to Fe^{3+}/Co^{3+} with increased temperature [41].

3.4. Electrical conductivity

Fig. 9 shows the temperature dependence of the conductivity of the PBCFC sample in air. Theoretical and experimental investigations reveal that oxygen ion transport in $LnBaCo_2O_{5+\delta}$ systems is anisotropic and transfers along the LnO and CoO_2 planes, whereas the BaO planes are a barrier for oxygen ion transport [42–44]. Considering that ion conductivity is much lower than electronic conductivity, the bulk conductivity measured for PBCFC is generally considered to be electronic conductivity. The electrical conductivity of the PBCFC sample initially increases and reaches a maximum

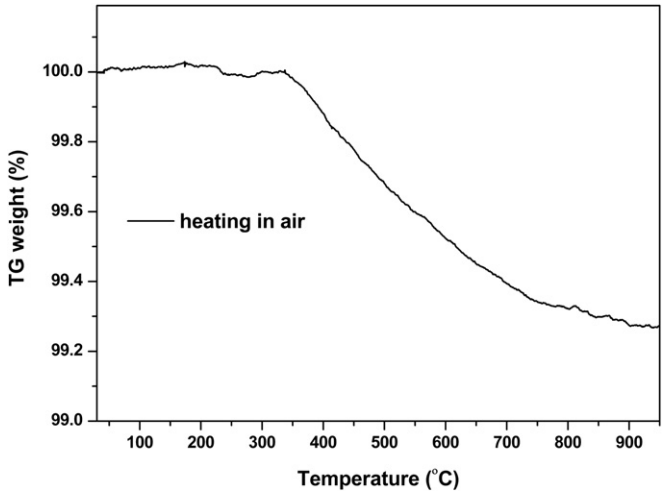

Fig. 8. TGA curve of the PBCFC sample in air.

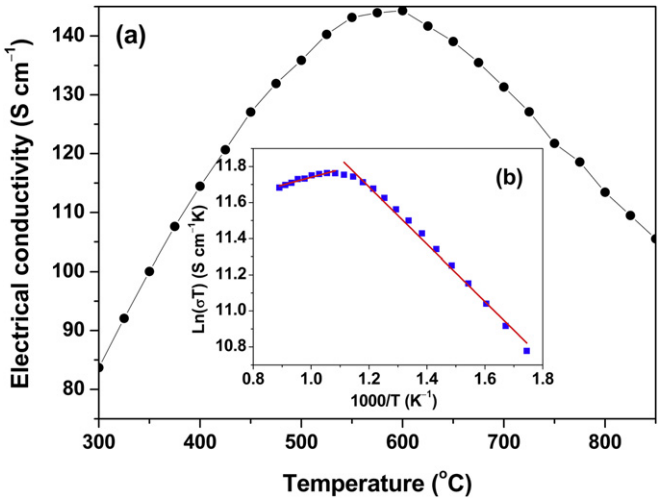

Fig. 9. Temperature dependence of the electrical conductivity of the PBCFC sample: (a) electrical conductivity vs. temperature and (b) $\ln(\sigma T)$ vs. $1000/T$.

value of 144 S cm^{-1} at 600 °C, and then decreases with further increased temperature. The sample exhibits semiconductor-like behavior at low temperatures, which follows a *p*-type small-polaron hopping mechanism through the transport of electron holes. The charge compensation for PBCFC is primarily electrons at low temperatures, and the conductivity can be attributed to the migration of electron holes. At high temperatures, the ionic compensation is dominant due to the loss of lattice oxygen with temperature, leading to a decrease in the oxygen content of the PBCFC. This result is in agreement with the TGA observation in Fig. 8. The increased concentration of oxygen vacancies decreases the concentration of electron holes [45]. Thus, the electrical conductivity decreases to show metallic-like behavior above 600 °C. Similar behaviors have also been reported in cobalt-based perovskite oxides [27,39,46–48]. Compared with PBCO and PBCF cathode materials, the introduction of Fe and Cu into PBCO obviously decreases the electrical conductivity of PBCFC. Zou et al. [27] reported the effect of Fe doping on the electrical conductivity of $PrBaCo_{2-x}Fe_xO_{5+\delta}$ materials. According to the XPS results, the lower valence states of the transition-metal cations can increase the concentration of oxygen vacancies. Furthermore, for PBCFC oxide, the introduction of 3d transition-metal cations of Fe and Cu perturbs the electron-hopping pathway along Co^{4+}–O^{2-}–Co^{3+}, leading to decreased electrical conductivity [27]. Nevertheless, the conductivity values of the PBCFC sample are 113–144 S cm^{-1} within the operating temperature range of IT-SOFCs. These values are higher than those of previously reported cobalt-based cathode materials [23,25,41].

Fig. 9(b) shows the Arrhenius plots of conductivity for the PBCFC sample. The $\ln(\sigma T)$ vs. $1000/T$ curve shows two linear behaviors at low and high temperatures. This result is mainly due to the abovementioned changes in electron hole and oxygen vacancy concentrations. The activation energies of electrical conductivities for small-polaron conduction calculated from the slope of the linear regressions at low and high temperatures are 13.2 and 3.61 kJ mol^{-1}, respectively.

3.5. Polarization resistance

To assess the electrochemical activity of PBCFC cathode, a symmetric cell configuration is used with SDC and GDC as electrolytes in air. Fig. 10(a) and (b) shows the typical impedance spectra of PBCFC cathode on SDC electrolyte at different calcining temperatures. Fig. 10 shows the right intercept on the Re*Z* axis representing

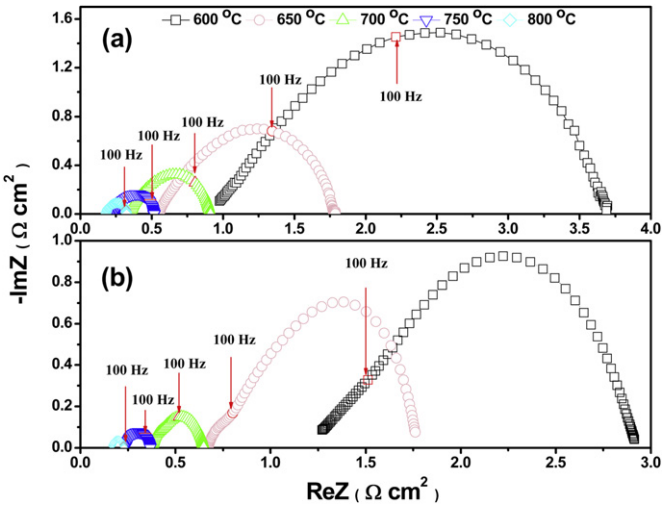

Fig. 10. Typical impedance spectra of PBCFC cathode on SDC electrolyte calcined at (a) 900 and (b) 950 °C.

the total resistance (R_{tot}) and the left intercept on the ReZ axis corresponding to the ohmic resistance (R_{ohm}, including the electrodes, electrolyte, current collectors, and lead wires). The polarization resistance R_p is estimated from the difference between R_{tot} and R_{ohm} ($R_p = R_{tot} - R_{ohm}$). As shown in Fig. 10, the calcining temperatures obviously affect the oxygen reduction reaction for PBCFC cathode. The polarization resistances significantly decrease with increased calcining temperature from 900 to 950 °C. The polarization resistances are 0.144 and 0.063 Ω cm^2 at 800 °C for the cathodes on SDC electrolyte calcined at 900 and 950 °C, respectively. Fig. 11 shows the Arrhenius plots of the polarization resistance for PBCFC cathode on SDC calcined at 900 and 950 °C, respectively. The activation energies are calculated to be 115.1 and 136.8 kJ mol^{-1} for PBCFC cathode on SDC calcined at 900 and 950 °C, respectively. Better adhesion between the cathode and electrolyte can be obtained at a calcining temperature of 950 °C compared with 900 °C. Therefore, the polarization resistance of the cathode calcined at 950 °C is lower than that at 900 °C. However, as confirmed by the XRD results in Section 3.1, PBCFC cathode is not chemically compatible with SDC electrolyte calcined at 950 °C for 10 h. To ensure the long-term stability of SOFCs, PBCFC cathode on SDC electrolyte should be calcined below 900 °C.

Fig. 12(a) shows the typical impedance spectra of PBCFC cathode on GDC electrolyte measured at 600–800 °C in air. The polarization resistance values are as low as 0.071 and 0.144 Ω cm^2 at 750 and 700 °C, respectively. These values are much lower than those of the PBCFC cathode on SDC electrolyte calcined at 900 and 950 °C. This finding indicates that PBCFC cathode on GDC electrolyte calcined at 950 °C may exhibit better electrocatalytic activity and interface adhesion. Fig. 12(b) shows the Arrhenius plot of the polarization resistance for PBCFC cathode on GDC electrolyte. The activation energy from the slope is calculated to be 118.9 kJ mol^{-1}. Compared with other cathodes under similar conditions, the polarization resistance of PBCFC cathode is lower than those of the double-perovskite cathode materials. For example, the polarization resistances are 0.165 and 0.184 Ω cm^2 at 700 °C for $LnBaCo_{2/3}Fe_{2/3}Cu_{2/3}O_{5+\delta}$ (Ln = Gd and Sm) cathodes on GDC electrolyte [24,40], and 0.330 Ω cm^2 at 800 °C for GBCCF cathode on GDC electrolyte [25]. Furthermore, the polarization resistance of the PBCFC cathode on GDC electrolyte is also lower than the target value of 0.15 Ω cm^2 at 700 °C as an IT-SOFC cathode [49]. This result implies that PBCFC cathode on GDC electrolyte has high electrocatalytic activity within the intermediate-temperature range.

3.6. Cell performance

Fig. 13 shows the I–V and I–P curves of the electrolyte-supported Ni–GDC/GDC/PBCFC cell, which is tested between 600 and 800 °C using dry H_2 as the fuel and ambient air as the oxidant. The OCV reaches 0.721, 0.798, 0.859, 0.906, and 0.933 V at 800, 750, 700, 650, and 600 °C, respectively. For the CeO_2-based electrolyte, the OCV is generally associated with several different factors, including gas leakage caused by sealing problems, possible electrolyte defects, and internal short circuits resulting from a reducing atmosphere [50]. Apart from other drawbacks, the decreased OCV values with increased temperature are mainly attributable to the partial reduction of Ce^{4+} to Ce^{3+} in GDC electrolyte under an anode atmosphere, resulting in the short circuiting of the internal electron conduction in GDC electrolyte. A lower OCV for GDC electrolyte cell with $PrBa_{0.5}Sr_{0.5}Co_2O_{5+\delta}$ cathode has also been previously reported, where the OCV is approximately 0.760 V at 800 °C [51]. The maximum power densities of the cell reach 659, 512, and 353 mW cm^{-2} at 800, 750, and

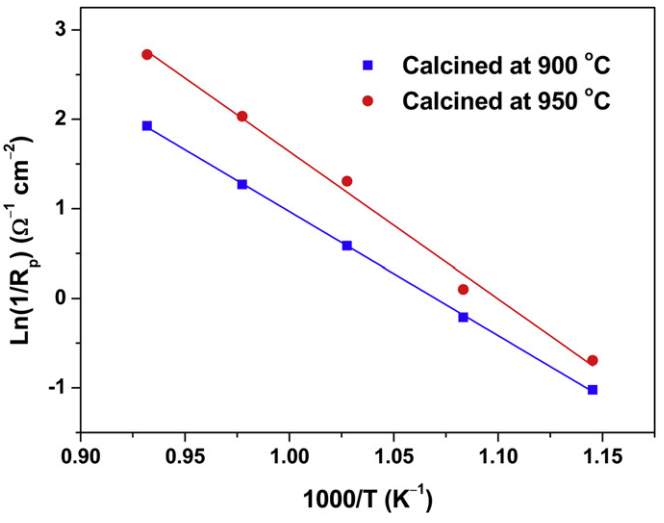

Fig. 11. Arrhenius plots of the polarization resistance for the PBCFC cathode on SDC electrolyte calcined at 900 and 950 °C.

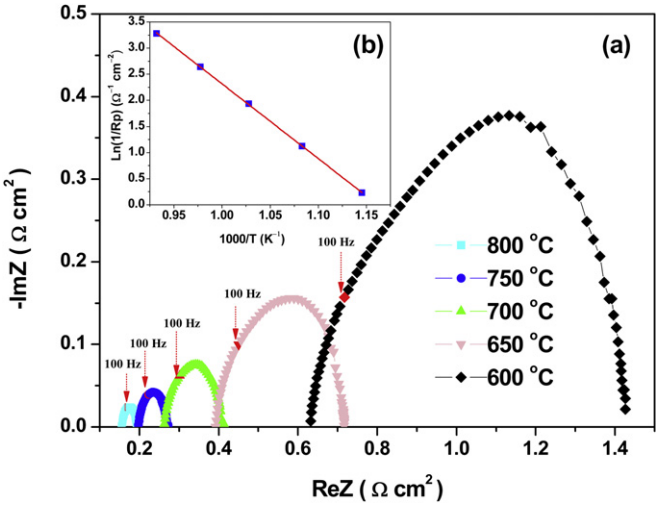

Fig. 12. (a) Typical impedance spectra of PBCFC cathode on GDC electrolyte calcined at 950 °C. (b) Arrhenius plots of the polarization resistance for PBCFC cathode on GDC electrolyte.

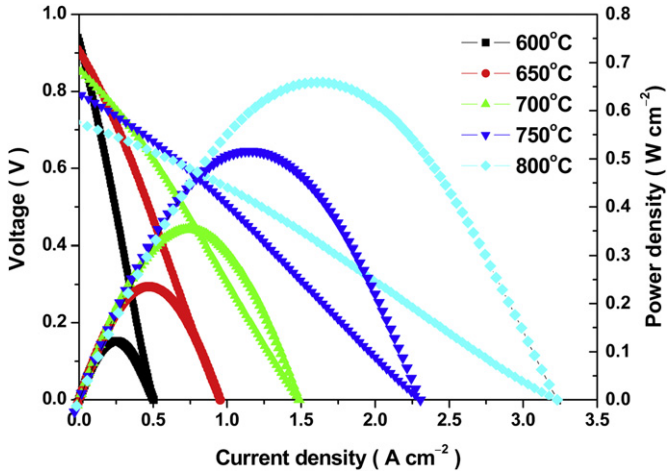

Fig. 13. Cell voltage and power density as a function of current density for an electrolyte-supported Ni–GDC/GDC/PBCFC cell under dry H_2 as the fuel and ambient air as the oxidant.

700 °C, respectively. PBCFC cathode shows improved cell performance compared with previously reported double-perovskite cathode materials. For example, a power density of 301 mW cm^{-2} at 700 °C has been reported for Ni–GDC/GDC/$PrBa_{0.5}Sr_{0.5}Co_2O_{5+\delta}$ cell [51]. These results demonstrate that the PBCFC material can be a high-performance cathode in GDC electrolyte IT-SOFCs.

4. Conclusions

A novel double-perovskite PBCFC is prepared by the EDTA–citrate complexing method, and evaluated as a potential cathode material for IT-SOFC applications. The XPS results indicate that the rare-earth and transition-metal cations in double-perovskite participate as mixed valence states of Pr^{3+}/Pr^{4+}, Fe^{3+}/Fe^{4+}, Co^{3+}/Co^{4+}, and Cu^{+}/Cu^{2+}. Compared with PBCO and PBCF cathodes, the substitution of Co by Fe and Cu in PBCO significantly reduces the TEC to 16.6×10^{-6} K^{-1} between 30 and 850 °C in air. The electrical conductivities of the PBCFC sample are 144–113 between 600 and 800 °C. The PBCFC material exhibits good chemical compatibility with GDC at 950 °C for 10 h and SDC at 900 °C for 10 h. The polarization resistance of PBCFC cathode on SDC electrolyte calcined at 900 °C cannot meet the requirement of the IT-SOFC cathode. Nevertheless, the polarization resistances for PBCFC cathode on GDC electrolyte are only 0.071 and 0.144 Ω cm^2 at 750 and 700 °C, respectively. The maximum power densities using PBCFC as cathode and GDC as electrolyte reach 659 and 512 mW cm^{-2} at 800 and 750 °C, respectively. The results indicate that double-perovskite PBCFC has potential use as a cathode material for GDC electrolyte IT-SOFCs.

Acknowledgments

This work was supported by the Natural Science Foundation of China under contract no. 10974065.

References

[1] N.Q. Minh, J. Am. Ceram. Soc. 76 (1993) 563–588.
[2] S.P. Jiang, J. Mater. Sci. 43 (2008) 6799–6833.
[3] N.P. Brandon, S. Skinner, B.C.H. Steele, Annu. Rev. Mater. Res. 33 (2003) 183–213.
[4] D.J.L. Brett, A. Atkinson, N.P. Brandon, S.J. Skinner, Chem. Soc. Rev. 37 (2008) 1568–1578.
[5] V.B. Vert, J.M. Serra, Fuel Cells 10 (2010) 693–702.
[6] Z.P. Shao, S.M. Haile, Nature 431 (2004) 170–173.
[7] A.V. Kovalevsky, V.V. Kharton, V.N. Tikhonovich, E.N. Naumovich, A.A. Tonoyan, O.P. Reut, L.S. Boginsky, Mater. Sci. Eng. B 52 (1998) 105–116.
[8] A. Esquirol, N.P. Brandon, J.A. Kilner, M. Mogensen, J. Electrochem. Soc. 151 (2004) A1847–A1855.
[9] A. Mai, V.A.C. Haanappel, S. Uhlenbruck, F. Tietz, D. Stöver, Solid State Ionics 176 (2005) 1341–1350.
[10] J.M. Serra, H.P. Buchkremer, J. Power Sources 172 (2007) 768–774.
[11] K. Zhang, L. Ge, R. Ran, Z.P. Shao, S.M. Liu, Acta Mater. 56 (2008) 4876–4889.
[12] Q.J. Zhou, F. Wang, Y. Shen, T.M. He, J. Power Sources 195 (2010) 2174–2181.
[13] Y.N. Kim, J.-H. Kim, A. Manthiram, J. Power Sources 195 (2010) 6411–6419.
[14] Q.J. Zhou, T.M. He, Y. Ji, J. Power Sources 185 (2008) 754–758.
[15] D.J. Chen, R. Ran, K. Zhang, J. Wang, Z.P. Shao, J. Power Sources 188 (2009) 96–105.
[16] A.A. Taskin, A.N. Lavrov, Y. Ando, Appl. Phys. Lett. 86 (2005) 091910-1–091910-3.
[17] G. Kim, S. Wang, A.J. Jacobson, L. Reimus, P. Brodersen, C.A. Mims, J. Mater. Chem. 17 (2007) 2500–2505.
[18] T. Ishihara, T. Kudo, H. Matsuda, Y. Takita, J. Electrochem. Soc. 142 (1995) 1519–1524.
[19] J.C. Burley, J.F. Mitchell, S. Short, D. Miller, Y. Tang, J. Solid State Chem. 170 (2003) 339–350.
[20] K. Asai, A. Yoneda, O. Yokokura, J.M. Tranquada, G. Shirane, K. kohn, J. Phys. Soc. Jpn. 67 (1998) 290–296.
[21] L. Qiu, T. Ichikawa, A. Hirano, N. Imanishi, Y. Takeda, Solid State Ionics 158 (2003) 55–65.
[22] L. Zhao, J.C. Shen, B.B. He, F.L. Chen, C.R. Xia, Int. J. Hydrogen Energy 36 (2011) 3658–3665.
[23] Q.J. Zhou, Y.C. Zhang, Y. Shen, T.M. He, J. Electrochem. Soc. 157 (2010) B628–B632.
[24] S.H. Jo, P. Muralidharan, D.K. Kim, Electrochem. Commun. 11 (2009) 2085–2088.
[25] Q.J. Zhou, T. Wei, S.Q. Guo, X.L. Qi, R.F. Ruan, Y. Li, H.Y. Yan, Q. Liu, Ceram. Int. 38 (2012) 2899–2903.
[26] J.-H. Kim, L. Mogni, F. Prado, A. Caneiro, J.A. Alonso, A. Manthiram, J. Electrochem. Soc. 156 (2009) B1376–B1382.
[27] J. Zou, J. Park, B. Kwak, H. Yoon, J. Chung, Solid State Ionics 206 (2012) 112–119.
[28] R.D. Shannon, Acta Cryst. A32 (1976) 751–767.
[29] H. Falcón, J.A. Barbero, G. Araujo, M.T. Casais, M.J. Martínez–Lope, J.A. Alonso, J.L.G. Fierro, Appl. Catal. B Environ. 53 (2004) 37–45.
[30] C. Abate, V. Esposito, K. Duncan, J.C. Nino, D.M. Gattia, E.D. Wachsman, E. Traversaz, J. Am. Ceram. Soc. 93 (2010) 1970–1977.
[31] H. He, H.X. Dai, K.W. Wong, C.T. Au, Appl. Catal. A 251 (2003) 61–74.
[32] M. Ghaffari, M. Shannon, H. Hui, O.K. Tan, A. Irannejad, Surf. Sci. 606 (2012) 670–677.
[33] J.C. Dupina, D. Gonbeau, H. Benqlilou-Moudden, Ph. Vinatier, A. Levasseur, Thin Solid Films 384 (2001) 23–32.
[34] E. Meza, J. Ortiz, D. Ruíz-León, J.F. Marco, J.L. Gautier, Mater. Lett. 70 (2012) 189–192.
[35] H. van der Heide, R. Hemmel, C.F. van Bruggen, C. Haas, J. Solid State Chem. 33 (1980) 17–25.
[36] M. O'Connell, A.K. Norman, C.F. HuÈttermann, M.A. Morris, Catal. Today 47 (1999) 123–132.
[37] T. Mathew, N.R. Shiju, K. Sreekumar, B.S. Rao, C.S. Gopinath, J. Catal. 210 (2002) 405–417.
[38] S. Poulston, P.M. Parlett, P. Stone, M. Bowker, Surf. Interface Anal. 24 (1996) 811–820.
[39] K.T. Lee, A. Manthiram, Chem. Mater. 18 (2006) 1621–1626.
[40] S.J. Lee, D.S. Kim, P. Muralidharan, S.H. Jo, D.K. Kim, J. Power Sources 196 (2011) 3095–3098.
[41] B. Wei, Z. Lü, S.Y. Li, Y.Q. Liu, K.Y. Liu, W.H. Su, Electrochem. Solid-State Lett. 8 (2005) A428–A431.
[42] D. Parfitt, A. Chroneos, A. Tarancón, J.A. Kilner, J. Mater. Chem. 21 (2011) 2183–2186.
[43] M. Burriel, J. Peña-Martínez, R.J. Chater, S. Fearn, A.V. Berenov, S.J. Skinner, J.A. Kilner, Chem. Mater. 24 (2012) 613–621.
[44] Y. Hu, O. Hernandez, T. Broux, M. Bahout, J. Hermet, A. Ottochian, C. Ritter, G. Geneste, G. Dezanneau, J. Mater. Chem. 22 (2012) 18744–18747.
[45] J.W. Stevenson, T.R. Armstrong, R.D. Carneim, L.R. Pederson, W.J. Weber, J. Electrochem. Soc. 143 (1996) 2722–2729.
[46] H. Takahashi, F. Munakata, M. Yamanaka, Phys. Rev. B 57 (1998) 15211–15218.
[47] Y. Shen, F. Wang, X. Ma, T.M. He, J. Power Sources 196 (2011) 7420–7425.
[48] H. Lü, Y.J. Wu, B. Huang, B.Y. Zhao, K. Hu, Solid State Ionics 177 (2006) 901–906.
[49] B.C.H. Steele, Solid State Ionics 86–88 (1996) 1223–1234.
[50] X.G. Zhang, M. Robertson, C. Deĉes–Petit, W. Qu, O. Kesler, R. Maric, D. Ghosh, J. Power Sources 164 (2007) 668–677.
[51] S.Q. Lü, G.H. Long, X.W. Meng, Y. Ji, B.R. Lü, H.Y. Zhao, Int. J. Hydrogen Energy 37 (2012) 5914–5919.